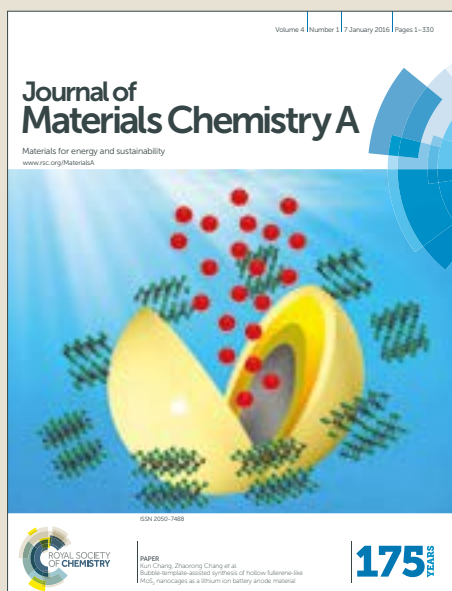


Journal of Materials Chemistry A

Accepted Manuscript



This article can be cited before page numbers have been issued, to do this please use: L. Han, T. Yu, W. Lei, W. Liu, K. Feng, Y. Ding, G. Jiang, P. Xu and Z. Chen, *J. Mater. Chem. A*, 2017, DOI: 10.1039/C7TA05146H.



This is an Accepted Manuscript, which has been through the Royal Society of Chemistry peer review process and has been accepted for publication.

Accepted Manuscripts are published online shortly after acceptance, before technical editing, formatting and proof reading. Using this free service, authors can make their results available to the community, in citable form, before we publish the edited article. We will replace this Accepted Manuscript with the edited and formatted Advance Article as soon as it is available.

You can find more information about Accepted Manuscripts in the [author guidelines](#).

Please note that technical editing may introduce minor changes to the text and/or graphics, which may alter content. The journal's standard [Terms & Conditions](#) and the ethical guidelines, outlined in our [author and reviewer resource centre](#), still apply. In no event shall the Royal Society of Chemistry be held responsible for any errors or omissions in this Accepted Manuscript or any consequences arising from the use of any information it contains.



Journal Name

COMMUNICATION

Nitrogen-doped Carbon Nanocones Encapsulating with Nickel–Cobalt Mixed Phosphides for Enhanced Hydrogen Evolution Reaction

Received 00th January 20xx,
Accepted 00th January 20xx

DOI: 10.1039/x0xx00000x

www.rsc.org/

Lei Han, Tongwen Yu, Wen Lei, Wenwen Liu, Kun Feng, Yuanli Ding, Gaopeng Jiang, Pan Xu and Zhongwei Chen*

In this work, nickel-cobalt mixed metal phosphides encapsulated into nitrogen-doped carbon nanocones (Ni₂P/NiCoP@NCCs) have been prepared through a facile ammonia-etching of nickel-cobalt Prussian blue analogs (Ni-Co PBA) followed by the subsequent phosphidation treatment. During the *in-situ* and confined phosphidation process, very small nickel-cobalt mixed metal phosphides nanocrystallites are uniformly incorporated into the simultaneously produced nitrogen-doped carbon matrix. Due to the unique structure and composition, the resultant Ni₂P/NiCoP@NCCs possesses high electrocatalytic activity and excellent durability for HER in both acidic and alkaline solutions.

Hydrogen production by electrochemical water splitting is widely regarded as a promising and attractive way to solve current energy crisis and environmental issues.^[1-8] In order to make this process efficient and practical, it is very necessary and important to exploit high active catalysts to accelerate hydrogen evolution reaction (HER). To date, the *state-of-the-art* HER electrocatalysts are mainly Pt-group noble metals and their alloy due to their high catalytic activity such as low overpotential and fast reaction kinetic.^[9-13] However, their paucity and high cost largely impede their practical applications. Fortunately, some transition-metal-based materials have been demonstrated as promising alternative to noble-metal HER electrocatalysts, including metal sulfides,^[14-15] metal carbides^[9-10], metal nitrides,^[16] and metal phosphides.^[17-21] Especially, transition-metal phosphides receive much more attention owing to their facile preparation and low-cost as well as excellent durability.^[4, 22-27] The performances of materials are largely related to their morphology.^[21, 28] Therefore, various methods have been developed to prepare different nanostructured morphologies of transition-metal phosphides, aiming to achieve optimal

performances.^[1-2, 22, 27, 29-30] As reported, the most efficient way to control the morphologies of transition-metal phosphides is to tune the morphology of the corresponding precursors. For instance, nanostructured cobalt oxides with different morphologies, including nanowires, nanosheets and nanoparticles, were firstly prepared and then converted into CoP *via* phosphidation route.^[31] In addition, cobalt phosphides with hollow and/or porous concave polyhedron structure have been successfully prepared by heat treatment of zeolitic imidazolate framework-67 (ZIF-67) polyhedron under air with the sequential phosphidation treatment with NaH₂PO₂.^[19, 32] Besides, Zhang et al. also reported the preparation of three-dimensional (3D) graphene aerogel decorated with cobalt phosphide nanoparticles through combining self-assembly with freeze-drying and thermal treatment as well as phosphidation process.^[17] Despite the progress, it still remains a challenge for the construction of transition-metal-phosphides precursors with special complex nanostructured morphologies such as nanocones because of their extreme formation condition needed.

In the past few years, chemical etching method has been reported as an efficient method to prepare some special complex nanostructures,^[28, 33-35] which can endow some unique physicochemical properties of materials themselves resulting from their novel nanostructures. Recently, Yamauchi's group and Lou's group utilized this method to prepare various Prussian blue analogues (PBAs) and/or PBA-derived metal oxides/sulfides with hollow complex nanostructures like hollow nanocubes, nanocages and nanoframes.^[28, 35-36] Inspired by them, in the present work, nickel-cobalt Prussian blue analogue (Ni-Co PBA) nanocones were successfully prepared through a facile ammonia-etching method (**Figure 1**). In the preparation procedure, we shorten the precipitation time of Ni-Co PBA nanocubes, thus achieving the successful preparation of Ni-Co PBA nanocones after ammonia-etching (see Supporting Information for experimental details). Finally, after the phosphidation treatment of the resultant Ni-Co PBA nanocones in Ar, nickel-cobalt mixed metal phosphides encapsulated into nitrogen-

Department of Chemical Engineering, University of Waterloo,
200 University Avenue West, Waterloo, Ontario, N2L3G1, Canada.
E-mail: zhwchen@uwaterloo.ca

*Electronic Supplementary Information (ESI) available: [details of any supplementary information available should be included here]. See DOI: 10.1039/x0xx00000x

COMMUNICATION

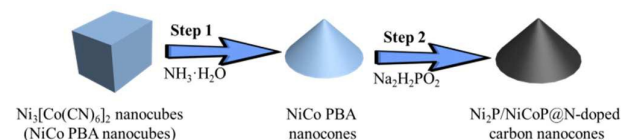


Figure 1 Schematic of the preparation of $\text{Ni}_2\text{P}/\text{NiCoP}@$ N-doped carbon nanocones (NCCs).

doped carbon nanocones ($\text{Ni}_2\text{P}/\text{NiCoP}@$ NCCs) could be obtained. It should be noted that in our work, Ni-Co PBA is chosen as precursor mainly based on the following two reasons. On one hand, as a typical metal-organic framework (MOF), Ni-Co PBA consists of Ni and Co, which makes it promising precursor to prepare bimetallic phosphides. Compared to monometallic phosphides, bimetallic phosphides provide two electron-donating active sites to facilitate the proton discharge in HER process, which helps in enhanced HER activity.^[37] On the other hand, active materials encapsulated into carbon matrix have been demonstrated as promising route to improve their HER activity because of the increase electronic conductivity, avoiding the aggregation and leaching of active materials, and the synergistic interaction between the encapsulated active materials and carbon matrix.^[10, 38-39] During the phosphidation process in our work, Ni-Co PBA can be easily converted into nickel-cobalt mixed metal phosphides encapsulated into nitrogen-doped carbon matrix. These features endow the high HER activity and excellent stability of the resultant $\text{Ni}_2\text{P}/\text{NiCoP}@$ NCCs.

Scanning electron microscope (SEM) and transmission electron microscopy (TEM) were firstly conducted to characterize the morphology and structure of the resultant Ni-Co PBA. As presented in **Figure 2a-b**, the resultant Ni-Co PBA exhibits cube morphology with uniform size of around 400 nm. The crystal structure of the resultant Ni-Co PBA nanotubes is investigated by X-ray diffraction (XRD). All XRD peaks (**Figure 2c**) can match well with phase-pure $\text{Ni}_3[\text{Co}(\text{CN})_6]_2 \cdot x\text{H}_2\text{O}$ (JCPDS card no. 89-3738). Energy dispersive X-ray (EDX) analysis result indicates that the composition of the resultant Ni-Co PBA nanocubes consist of Ni, Co, C, and N (**Figure S1a**), which is consistent with the XRD result. After reacting with ammonia solution for 1 h at room temperature, the resultant Ni-Co PBA nanocubes are interestingly converted into cone-like nanoparticles (**Figure 2d-f**). It can be seen from **Figure 2d-e** that the resultant Ni-Co PBA after ammonia-etching exhibits uniform nanocones morphology. TEM images (**Figure 2f**) also confirm the successful formation of cone-like nanostructures. The composition and crystalline phase of the resultant Ni-Co PBA nanocones are also confirmed by EDX analysis and XRD. As seen, the molar ratio of Ni and Co remains the similar as that of the precursor nanocubes (**Figure S1b**), and we also interestingly find that all diffraction peaks are also the same as that of the precursor nanocubes (**Figure 2c**), which are in accordance with our previous reported results.^[28] The formation of the unique nanostructures could be explained as follows. As we know, the chemical etching process easily happens along with the defect-rich region, and its rate largely

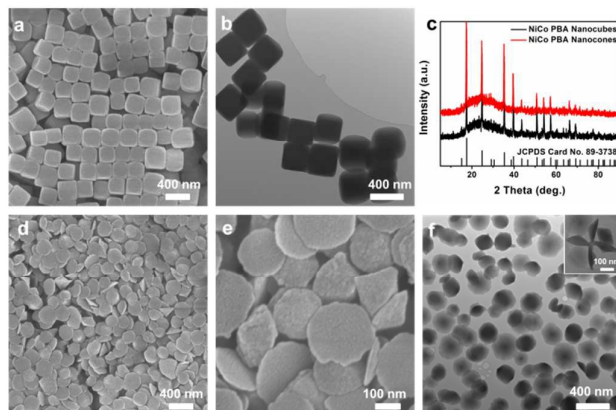


Figure 2 (a, d-e) SEM images, (b, f) TEM images and (c) Powder XRD patterns of the resultant NiCo PBA nanocubes (a-c) and NiCo PBA nanocones (c-f).

depends on the density of defects.^[28] In comparison to the flat planes, the corners of the cubes were reported to expose more defects. In addition, the formation of Ni-Co PBA nanocubes is the result of Ostwald ripening, which results in the interior defect-rich parts along the diagonals of the cubes.^[28] So when reacting with ammonia, the cubes are initially etched at their eight corners. As the reaction time prolongs, the diagonal of the cubes begin to be etched, and finally nanocones are obtained with twelve edges vanish.

The resultant Ni-Co PBA nanocones were further heat-treated with NaH_2PO_2 under Ar. The morphology and structure of the resultant $\text{Ni}_2\text{P}/\text{NiCoP}@$ NCCs are characterized by SEM and TEM, and the results are shown in **Figure 3**. It can be seen that the nanocones nanostructures are well maintained in the resultant $\text{Ni}_2\text{P}/\text{NiCoP}@$ NCCs (**Figure 3a-c**). The high-resolution TEM images (**Figure 3d-e**) indicate that very small $\text{Ni}_2\text{P}/\text{NiCoP}$ nanoparticles are successfully uniformly encapsulated into the produced continuous carbon matrix. The scanning TEM and EDX mapping were also carried out to unravel the morphology and element distribution. It can be easily observed that the four elements including C, Ni, Co, and P are uniformly distributed in the resultant $\text{Ni}_2\text{P}/\text{NiCoP}@$ NCCs (**Figure 3f-j**),

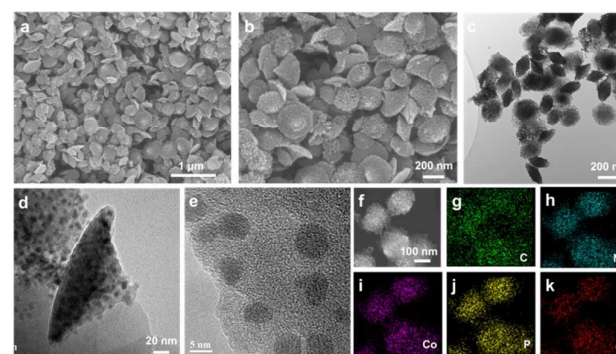


Figure 3 (a-b) SEM images, (c-d) TEM images, (e) HRTEM, and (f) HAADF-STEM and (g-k) elemental mapping images of the resultant $\text{Ni}_2\text{P}/\text{NiCoP}@$ NCCs.

which is in accordance with EDX result (Figure S1d). XRD pattern reveals that the resultant product after phosphidation treatment consists of Ni_2P (JCPDS card no. 89-2742) and NiCoP (JCPDS card no. 71-2336) (Figure S3), and no peaks corresponding to NiCo_2O_4 were observed. Besides, there is a broad diffraction peak at 25° , which can be assigned to the (002) plane of the hexagonal graphitic structure of carbon.^[40] The Raman spectra result (Figure S4) also confirms the existence of carbon, where there are two bands centered at 1340 and 1555 cm^{-1} related to the disorders of the graphite (D-band) and the sp^2 carbon bonded graphitic structures (G-band), respectively.^[40] As comparison, the resultant Ni-Co PBA nanocubes were also directly heat-treated with NaH_2PO_2 under Ar. SEM and TEM images reveal that the resultant product retains well cube morphology with hollow structures (Figure S2). Besides, XRD result confirms its composition also contains Ni_2P and NiCoP (Figure S3). Hereafter this product is labeled as $\text{Ni}_2\text{P}/\text{NiCoP}@\text{NHCCs}$ for simplicity's sake.

XPS spectra were further carried out to analyze the surface elemental composition and the valence states in the resultant $\text{Ni}_2\text{P}/\text{NiCoP}@\text{NHCCs}$. The XPS survey spectra in Figure S5a shows the existence of Co, Ni, P, C, N, and O elements in the resultant $\text{Ni}_2\text{P}/\text{NiCoP}@\text{NHCCs}$. The high-resolution XPS spectra of Co 2p, Ni 2p, P 2p, C 1s, N 1s, and O 1s are shown in Figure S5b–g. In Co 2p spectra (Figure S5b), peaks at 778.9 and 781.9 eV are assigned to $\text{Co } 2\text{p}_{3/2}$, while the peak located at 786.1 eV is ascribed to the satellite peak of $\text{Co } 2\text{p}_{3/2}$. The $\text{Co } 2\text{p}_{1/2}$ region also shows two main peaks at 793.5 and 798.1 eV and one satellite peak at 803 eV. For $\text{Co } 2\text{p}_{3/2}$, the peak at 778.9 eV belongs to Co-P. The peak at 781.9 eV could be attributed to a Co oxidized state, which is related to Co-PO_x . In Ni 2p spectra (Figure S5c), the peaks at 856.9 eV and 861.6 eV are assigned to the oxidized Ni species and the satellite of the $\text{Ni } 2\text{p}_{3/2}$, respectively. The other peaks at 874.8 eV and 880.2 eV correspond to oxidized Ni species, and the satellite of the $\text{Ni } 2\text{p}_{1/2}$, respectively. As shown in Figure S5d, there are two peaks at 129.3 eV and 134 eV in P 2p spectra, which stand for reduced phosphorus in metal phosphides and phosphate species resulting from the oxidation of metal phosphides after exposure to air, respectively. To further demonstrate the oxidized Co/Ni, the O 1s binding energy is shown in Figure S5g. As shown, there are also two peaks at 531.5 eV and 533 eV, which belongs to either MO_x or M(OH)_x ($\text{M} = \text{Co, Ni}$) and oxidized phosphate species, respectively. Figure S5f shows the XPS spectra of N 1s, where the peaks at 398.9, 400, and 401 eV can be attributed to pyridinic-N, pyrrolic-N, and quaternary-N, respectively. C 1s spectra (Figure S5e) also shows three peaks at 284.6, 286.2, and 288.9 eV, which are ascribed to $\text{sp}^2\text{-C}$, -C-O- , and -C=O , respectively. All of these XPS data confirm the successful synthesis of $\text{Ni}_2\text{P}/\text{NiCoP}@\text{NHCCs}$.

The HER activities of the resultant products including $\text{Ni}_2\text{P}/\text{NiCoP}@\text{NCCs}$ and $\text{Ni}_2\text{P}/\text{NiCoP}@\text{NHCCs}$ were evaluated in a three-electrode configuration, where graphite rod and saturated calomel electrode (SCE) are used as counter electrode and reference electrode, respectively. The effect of loading amount of the catalyst on the HER activity was firstly investigated. It can be clearly noticed from Figure S6 that the

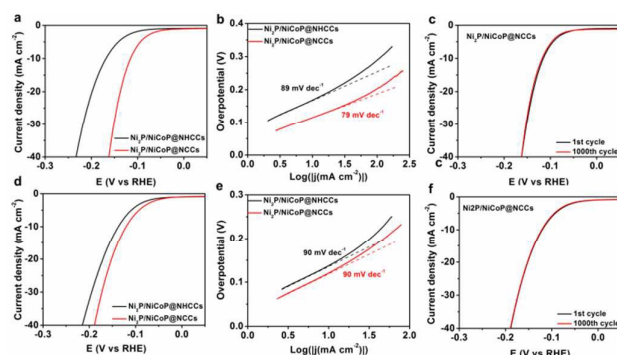


Figure 4 Electrochemical evaluation of the resultant $\text{Ni}_2\text{P}/\text{NiCoP}@\text{NHCCs}$ and $\text{Ni}_2\text{P}/\text{NiCoP}@\text{NCCs}$ in 1.0 M NaOH (a-c) and 0.5 M H_2SO_4 (d-f) with loading amount of 0.5 mg cm^{-2} : (a-d) Polarization curves with iR-corrected) on the GC electrode at 5 mV s^{-1} , (b-e) Tafel slopes, and (c-f) Polarization curves with iR-corrected) of $\text{Ni}_2\text{P}/\text{NiCoP}@\text{NCCs}$ before and after 1000 cycles at a scan rate of 100 mV s^{-1} between 0.05 V and -0.233 V.

resultant $\text{Ni}_2\text{P}/\text{NiCoP}@\text{NCCs}$ exhibits the highest HER activity when the loading amount is 0.5 mg cm^{-2} . Therefore the loading amount is fixed at 0.5 mg cm^{-2} in the later experiment. Then we compared the HER activity of the resultant $\text{Ni}_2\text{P}/\text{NiCoP}@\text{NCCs}$ and $\text{Ni}_2\text{P}/\text{NiCoP}@\text{NHCCs}$. Figure 4a exhibits the polarization curves of the resultant $\text{Ni}_2\text{P}/\text{NiCoP}@\text{NCCs}$ and $\text{Ni}_2\text{P}/\text{NiCoP}@\text{NHCCs}$ in 1.0 M KOH. Obviously, the resultant $\text{Ni}_2\text{P}/\text{NiCoP}@\text{NCCs}$ shows the lower onset potential and higher current density towards HER than the resultant $\text{Ni}_2\text{P}/\text{NiCoP}@\text{NHCCs}$. Specially, at a current density of 10 mA cm^{-2} , the overpotential for the resultant $\text{Ni}_2\text{P}/\text{NiCoP}@\text{NCCs}$ (116 mV) is lower as 52 mV than that of the resultant $\text{Ni}_2\text{P}/\text{NiCoP}@\text{NHCCs}$ (168 mV). Moreover, the HER performance is superior to that of other reported bimetallic phosphides such as NiCoP hollow polyhedra and $\text{CuCoP}/\text{nitrogen-doped carbon}$ (see Table S1).^[18, 20] At the same time, the kinetic behaviors of the resultant $\text{Ni}_2\text{P}/\text{NiCoP}@\text{NCCs}$ and $\text{Ni}_2\text{P}/\text{NiCoP}@\text{NHCCs}$ are also further investigated by Tafel plots derived from Figure 4a according to the Tafel equation ($\eta = b \log j + a$, where η is the overpotential, j is the current density, and b is the Tafel slope). As displayed in Figure 4b, the Tafel slope of the resultant $\text{Ni}_2\text{P}/\text{NiCoP}@\text{NCCs}$ (79 mV dec^{-1}) is slightly smaller than that of the resultant $\text{Ni}_2\text{P}/\text{NiCoP}@\text{NHCCs}$ (89 mV dec^{-1}), indicating the improved HER kinetic over the resultant $\text{Ni}_2\text{P}/\text{NiCoP}@\text{NCCs}$. As for stability, it is also important for practical application. So recycling CV or LSV experiment was performed to evaluate the stability of the resultant catalysts. Figure 4c shows the polarization curves of the resultant $\text{Ni}_2\text{P}/\text{NiCoP}@\text{NCCs}$ before and after 1000 continuous cyclic voltammetry (CV) cycles at a scan rate of 100 mV s^{-1} between 0.05 V and -0.257 V (vs. RHE). No obvious change of HER activity is observed, revealing the good stability of the resultant $\text{Ni}_2\text{P}/\text{NiCoP}@\text{NCCs}$. On the other hand, the HER activity of the resultant catalysts was also evaluated in 0.5 M H_2SO_4 , and the results are displayed in Figure 4d-f. The HER activity of the resultant

Ni₂P/NiCoP@NCCs also outperforms obviously that of the resultant Ni₂P/NiCoP@NHCCs, including lower onset potential and higher current density (Figure 4d). The overpotential of 120 mV the resultant Ni₂P/NiCoP@NCCs is only required to achieve the current density of 10 mA cm⁻², which is lower than that of the resultant Ni₂P/NiCoP@NHCCs (136 mV) and outperforms the reported other metal phosphides such as porous CoP concave polyhedron and porous Ni₂P polyhedrons (see Table S1).^[19, 41] Figure 4e displays the Tafel plot of the resultant Ni₂P/NiCoP@NCCs and Ni₂P/NiCoP@NHCCs, where the same Tafel slope (79 mV dec⁻¹) can be observed. Moreover, the resultant Ni₂P/NiCoP@NCCs also possesses good stability in 0.5 M H₂SO₄ (Figure 4f). Generally, HER process involves the following steps in acidic solution: the Volmer step (116 mV dec⁻¹), the Heyrovsky step (38 mV dec⁻¹), or the Tafel step (29 mV dec⁻¹).^[49] Therefore, the Tafel slope of the resultant Ni₂P/NiCoP@NCCs indicates that the corresponding HER follows a Volmer–Heyrovsky mechanism. However, the large Tafel slope herein may be further optimized by annealing temperature and the mass ratio of NiCo PBA and NaH₂PO₂.

In order to get insight for enhanced HER activity, we firstly measured the Brunauer-Emmett-Teller (BET) surface area (Figure S7). As can be noted, the BET surface area of the resultant Ni₂P/NiCoP@NCCs (67.3 m² g⁻¹) is higher than that of the resultant Ni₂P/NiCoP@NHCCs (29.2 m² g⁻¹), which is beneficial for improving the HER activity. Then electrochemical impedance spectroscopy (EIS) was also performed to investigate the interfacial behavior of the resultant Ni₂P/NiCoP@NCCs and Ni₂P/NiCoP@NHCCs modified electrodes (Figure S8). It can be seen that the resultant Ni₂P/NiCoP@NCCs shows the smaller electron-transfer resistance than the resultant Ni₂P/NiCoP@NHCCs, which may help to enhance the HER activity. Finally electrochemical active surface area (ECSA) was estimated according to the electrochemical double-layer capacitance (C_{dl}).^[28] Based on this point, CV curves with different scan rate in the potential range without the redox process were carried out. As presented in Figure S9 and Figure S10, the resultant Ni₂P/NiCoP@NCCs and Ni₂P/NiCoP@NHCCs both have almost same ECSA. Therefore, the enhanced HER activity could be attributed to the synergistic effect of the large BET surface area and small electron-transfer resistance.

In summary, we have successfully prepared Ni₂P/NiCoP@NCCs through a facile ammonia-etching and phosphidation treatment using Ni-Co PBA nanocubes as precursor. The *in-situ* and confined phosphidation process leads to the formation of very small Ni₂P/NiCoP nanocrystallites encapsulated uniformly into the generated nitrogen-doped carbon matrix. When used as HER electrocatalysts, the resultant Ni₂P/NiCoP@NCCs exhibits high electrocatalytic activity in both alkaline and acidic solutions with low overpotential at current density of 10 mA cm⁻² and good stability owing to the unique structure and morphology.

Acknowledgement

This research was supported by the Natural Sciences and Engineering Research Council of Canada (NSERC). TEM was obtained at the Canadian Center for Electron Microscopy (CEEM) located at McMaster University.

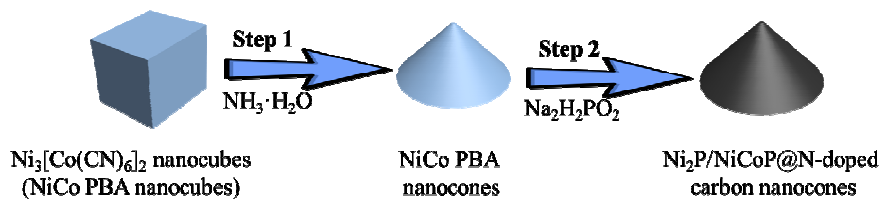
Notes and references

- H. Yang, Y. Zhang, F. Hu, Q. Wang, *Nano Lett.* **2015**, *15*, 7616-7620.
- R. Zhang, X. Wang, S. Yu, T. Wen, X. Zhu, F. Yang, X. Sun, W. Hu, *Adv. Mater.* **2017**, *29*, 1605502.
- M. A. R. Anjum, J. S. Lee, *ACS Catal.* **2017**, *7*, 3030-3038.
- P. Xiao, W. Chen, X. Wang, *Adv. Energy Mater.* **2015**, *5*, 1500985.
- D. Li, H. Baydoun, C. N. Verani, S. L. Brock, *J. Am. Chem. Soc.* **2016**, *138*, 4006-4009.
- P. He, X. Y. Yu, X. W. Lou, *Angew. Chem. Int. Ed.* **2017**, *56*, 3897-3900.
- G. Li, X. Wang, M. H. Seo, S. Hemmati, A. Yu, Z. Chen, *J. Mater. Chem. A* **2017**, DOI: 10.1039/C7TA02745A.
- W. Gu, L. Gan, X. Zhang, E. Wang, J. Wang, *Nano Energy* **2017**, *34*, 421-427.
- B. Sljukic, D. M. Santos, M. Vujkovic, L. Amaral, R. P. Rocha, C. A. Sequeira, J. L. Figueiredo, *ChemSusChem* **2016**, *9*, 1200-1208.
- L. Han, M. Xu, Y. Han, Y. Yu, S. Dong, *ChemSusChem* **2016**, *9*, 2784-2787.
- W. Hong, J. Wang, E. Wang, *Small* **2014**, *10*, 3262-3265.
- W. Hong, C. Shang, J. Wang, E. Wang, *Energy Environ. Sci.* **2015**, *8*, 2910-2915.
- W. Hong, J. Wang, E. Wang, *ACS Appl. Mater. Interfaces* **2014**, *6*, 9481-9487.
- C. G. Morales-Guio, X. Hu, *Acc. Chem. Res.* **2014**, *47*, 2671-2681.
- L. Lin, N. Miao, Y. Wen, S. Zhang, P. Ghosez, Z. Sun, D. A. Allwood, *ACS Nano* **2016**, *10*, 8929-8937.
- L. Han, K. Feng, Z. Chen, *Energy Tech.* **2017**, DOI: 10.1002/ente.201700108.
- X. Zhang, Y. Han, L. Huang, S. Dong, *ChemSusChem* **2016**, *9*, 3049-3053.
- J. Song, C. Zhu, B. Z. Xu, S. Fu, M. H. Engelhard, R. Ye, D. Du, S. P. Beckman, Y. Lin, *Adv. Energy Mater.* **2017**, *7*, 1601555.
- M. Xu, L. Han, Y. Han, Y. Yu, J. Zhai, S. Dong, *J. Mater. Chem. A* **2015**, *3*, 21471-21477.
- Y. Li, J. Liu, C. Chen, X. Zhang, J. Chen, *ACS Appl. Mater. Interfaces* **2017**, *9*, 5982-5991.
- L. Han, S. Dong, E. Wang, *Adv. Mater.* **2016**, *28*, 9266-9291.
- T. Wu, M. Pi, D. Zhang, S. Chen, *J. Power Sources* **2016**, *328*, 551-557.
- Z. Jin, P. Li, X. Huang, G. Zeng, Y. Jin, B. Zheng, D. Xiao, *J. Mater. Chem. A* **2014**, *2*, 18593-18599.
- C. Deng, F. Ding, X. Li, Y. Guo, W. Ni, H. Yan, K. Sun, Y.-M. Yan, *J. Mater. Chem. A* **2016**, *4*, 59-66.
- H. Du, Q. Liu, N. Cheng, A. M. Asiri, X. Sun, C. M. Li, *J. Mater. Chem. A* **2014**, *2*, 14812.
- X. Wang, W. Yuan, Y. Yu, C. M. Li, *ChemSusChem* **2017**, *10*, 1014-1021.
- Y. Bai, L. Fang, H. Xu, X. Gu, H. Zhang, Y. Wang, *Small* **2017**, *13*, 1603718.
- L. Han, X. Y. Yu, X. W. Lou, *Adv. Mater.* **2016**, *28*, 4601-4605.
- Y. Feng, X. Y. Yu, U. Paik, *Chem. Commun.* **2016**, *52*, 1633-1636.
- Y. Bai, H. Zhang, L. Liu, H. Xu, Y. Wang, *Chem. Eur. J.* **2016**, *22*, 1021-1029.

Journal Name

COMMUNICATION

- 31 P. Jiang, Q. Liu, C. Ge, W. Cui, Z. Pu, A. M. Asiri, X. Sun, *J. Mater. Chem. A* **2014**, *2*, 14634.
- 32 M. Liu, J. Li, *ACS Appl. Mater. Interfaces* **2016**, *8*, 2158-2165.
- 33 X. Xu, Z. Zhang, X. Wang, *Adv. Mater.* **2015**, *27*, 5365-5371.
- 34 M. Hu, S. Furukawa, R. Ohtani, H. Sukegawa, Y. Nemoto, J. Reboul, S. Kitagawa, Y. Yamauchi, *Angew. Chem. Int. Ed.* **2012**, *51*, 984-988.
- 35 M. Hu, N. L. Torad, Y. Yamauchi, *Eur. J. Inorg. Chem.* **2012**, *2012*, 4795-4799.
- 36 X. Y. Yu, L. Yu, H. B. Wu, X. W. Lou, *Angew. Chem. Int. Ed.* **2015**, *54*, 5331-5335.
- 37 J. Hao, W. Yang, Z. Zhang, J. Tang, *Nanoscale* **2015**, *7*, 11055-11062.
- 38 Z. Pu, X. Ya, I. S. Amiin, Z. Tu, X. Liu, W. Li, S. Mu, *J. Mater. Chem. A* **2016**, *4*, 15327-15332.
- 39 Y. P. Zhu, X. Xu, H. Su, Y. P. Liu, T. Chen, Z. Y. Yuan, *ACS Appl. Mater. Interfaces* **2015**, *7*, 28369-28376.
- 40 R. Jia, J. Chen, J. Zhao, J. Zheng, C. Song, L. Li, Z. Zhu, *J. Mater. Chem.* **2010**, *20*, 10829.
- 41 L. Yan, P. Dai, Y. Wang, X. Gu, L. Li, L. Cao, X. Zhao, *ACS Appl. Mater. Interfaces* **2017**, *9*, 11642-11650.



Nickel-cobalt mixed metal phosphides encapsulated into nitrogen-doped carbon nanocones have been successfully prepared through a facile ammonia-etching method with the subsequent phosphidation treatment, which exhibit excellent high electro-catalytic activity and excellent stability toward hydrogen evolution reaction in both acidic and alkaline solutions.